

## Hydrazylpyridine salicylaldehyde-copper(II)-1,10-phenanthroline complexes as potential anticancer agents: synthesis, characterization and anticancer evaluation

Yating Chen,<sup>a,b</sup> Zhilin Ke,<sup>a,b</sup> Lingyu Yuan,<sup>a</sup> Meixiang Liang,<sup>\*,a</sup> Shuhua Zhang<sup>\*,a,b</sup>  
<sup>a</sup>Guangxi Key Laboratory of Electrochemical and Magnetochemical Functional Materials, College of Materials Science and Engineering, Guilin University of Technology, Guilin, 541004, P R China. E-mail: [zsh720108@163.com](mailto:zsh720108@163.com) (Zhang S.), [39598671@qq.com](mailto:39598671@qq.com) (liang M.)  
<sup>b</sup>College of Chemistry, Guangdong University of Petrochemical Technology, Maoming, Guangdong, 525000, P R China.

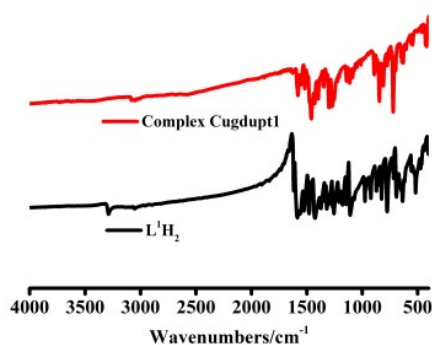


Fig. S1. IR (KBr) spectra of **Cugdup1** and **L<sup>1</sup>H<sub>2</sub>**.

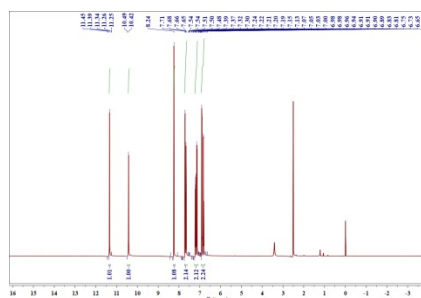
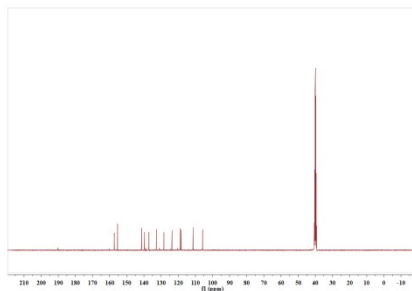
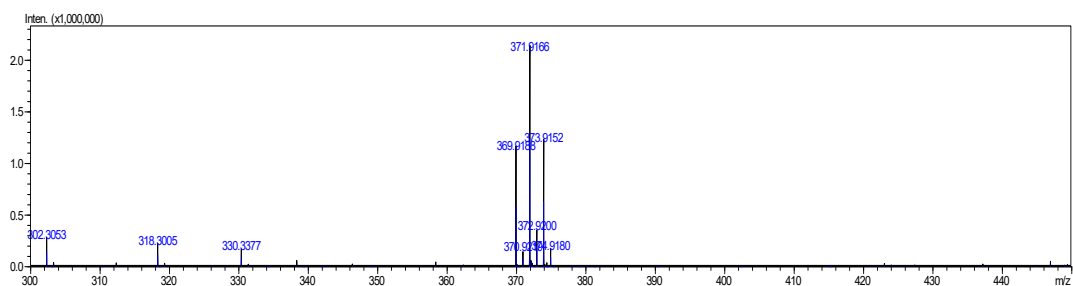


Fig. S2. <sup>1</sup>H NMR (500MHz, DMSO-d<sub>6</sub>) for **L<sup>1</sup>H<sub>2</sub>**.



**Fig. S3.**  $^{13}\text{C}$  NMR (400MHz, DMSO- $d_6$ ) for  $\text{L}^1\text{H}_2$ .



**Fig. S4.** ESI-MS spectra of  $\text{L}^1\text{H}_2$ .

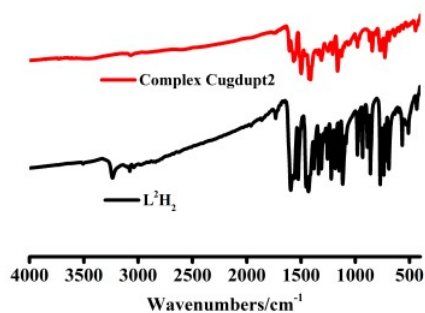


**Fig. S5.** IR (KBr) spectra of Cugdupt2 and  $\text{L}^2\text{H}_2$ .

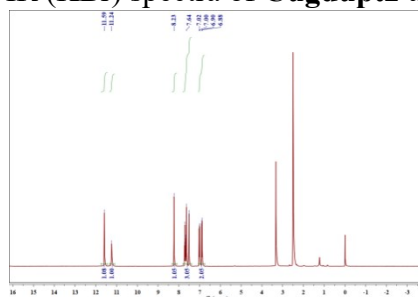


**Fig. S6.**  $^1\text{H}$  NMR (400MHz, DMSO- $d_6$ ) for  $\text{L}^2\text{H}_2$ .

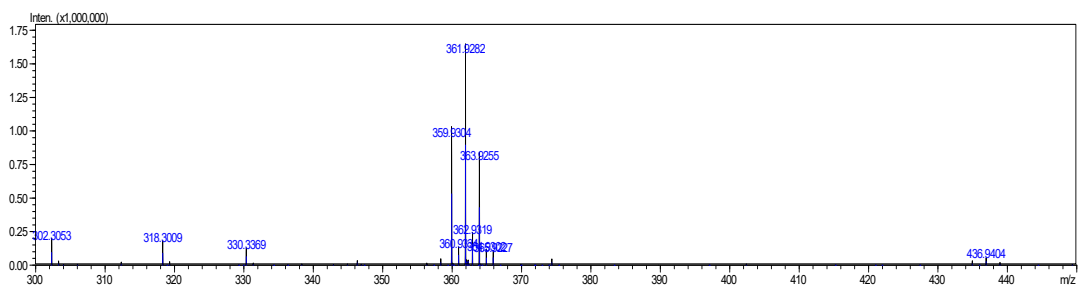


**Fig. S7.** ESI-MS spectra of  $\text{L}^2\text{H}_2$ .

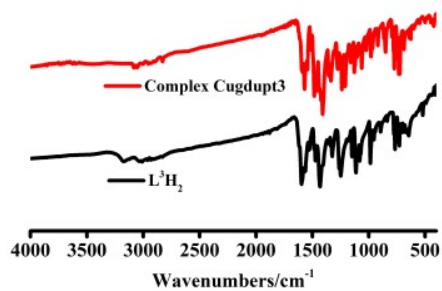


Fig. S8. IR (KBr) spectra of Cugdupt3 and L<sup>3</sup>H<sub>2</sub>.

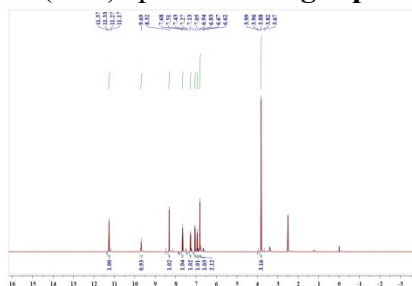


Fig. S9. <sup>1</sup>H NMR (500MHz, DMSO-d<sub>6</sub>) for L<sup>3</sup>H<sub>2</sub>.

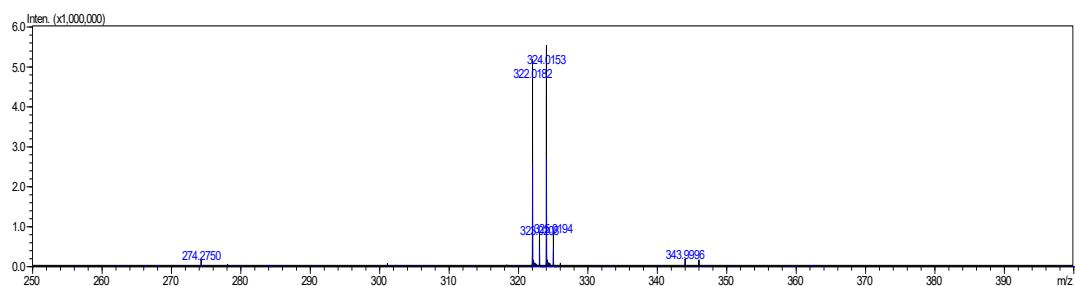


Fig. S10. ESI-MS spectra of L<sup>3</sup>H<sub>2</sub>.

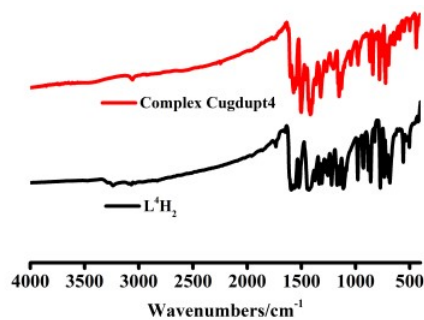


Fig. S11. IR (KBr) spectra of Cugdupt4 and L<sup>4</sup>H<sub>2</sub>.

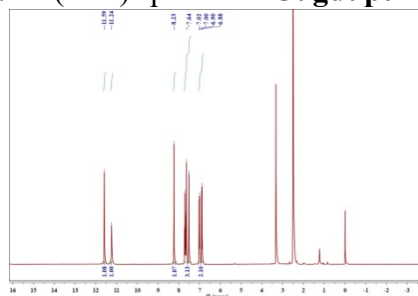
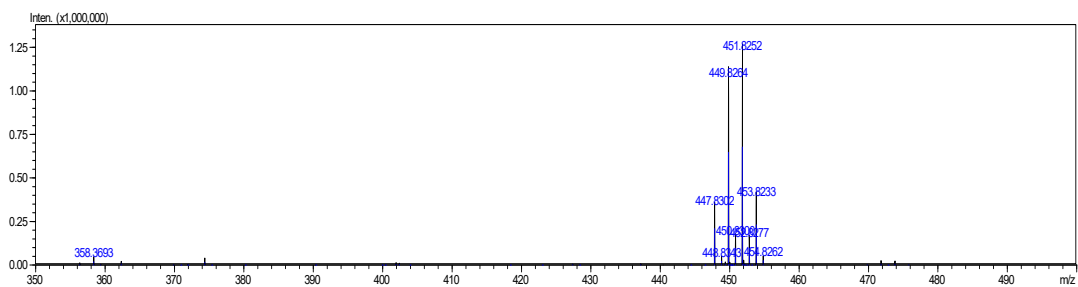
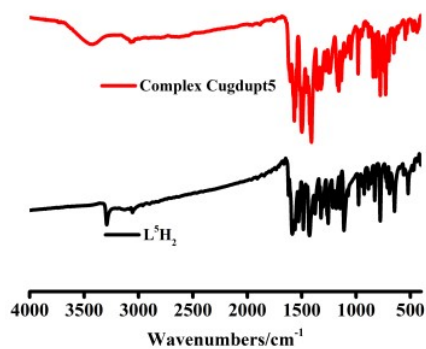


Fig. S12. <sup>1</sup>H NMR (400MHz, DMSO-d<sub>6</sub>) for L<sup>4</sup>H<sub>2</sub>.



**Fig. S13.** ESI-MS spectra of  $L^4H_2$ .



**Fig. S14.** IR (KBr) spectra of **Cugdup5** and  $L^5H_2$ .

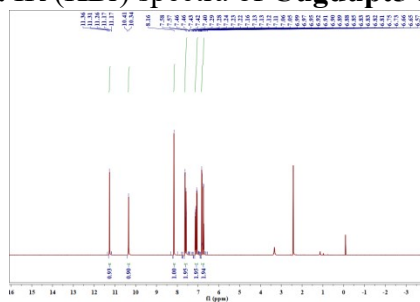


**Fig. S15.**  $^1H$  NMR (500MHz, DMSO- $d_6$ ) for  $L^5H_2$ .

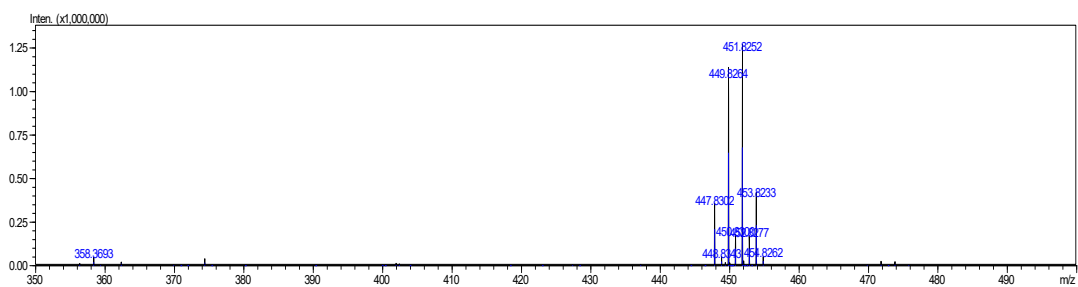


**Fig. S16.** ESI-MS spectra of  $L^5H_2$ .

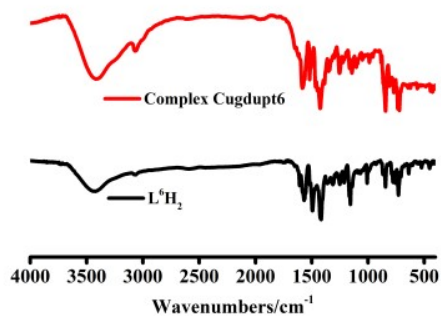


**Fig. S17.** IR (KBr) spectra of **Cugdup6** and  $L^6H_2$ .

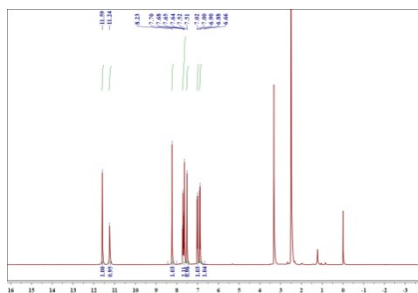


Fig. S18.  $^1\text{H}$  NMR (400MHz, DMSO- $d_6$ ) for  $\text{L}^6\text{H}_2$ .

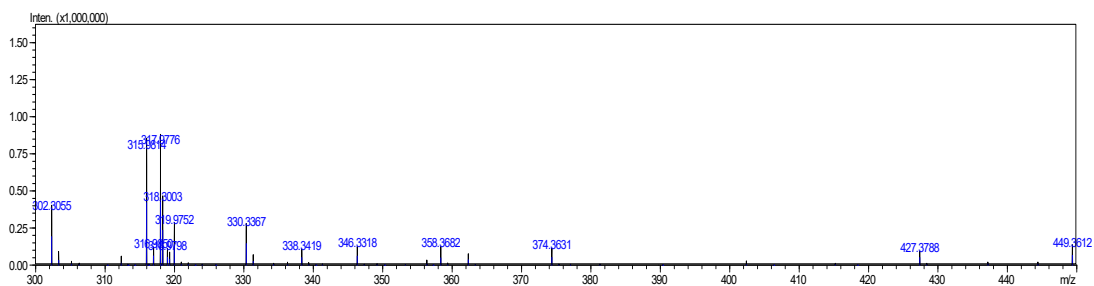


Fig. S19. ESI-MS spectra of  $\text{L}^6\text{H}_2$ .

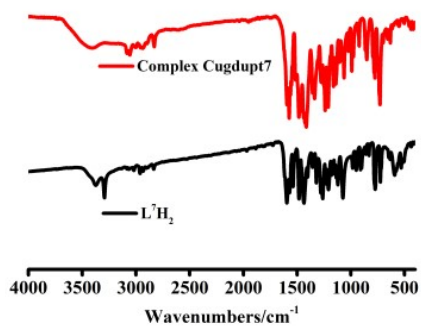


Fig. S20. IR (KBr) spectra of Cugdup7 and  $\text{L}^7\text{H}_2$ .

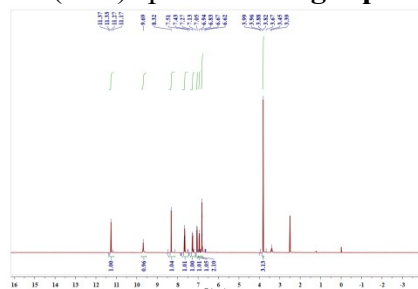


Fig. S21.  $^1\text{H}$  NMR (500MHz, DMSO- $d_6$ ) for  $\text{L}^7\text{H}_2$ .

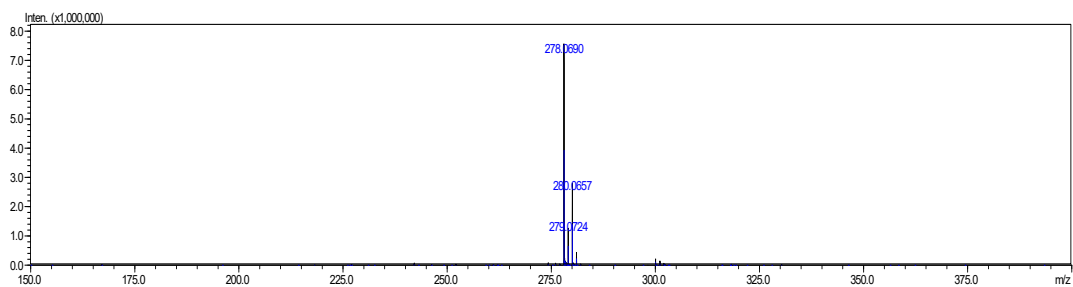


Fig. S22. ESI-MS spectra of  $\text{L}^7\text{H}_2$ .

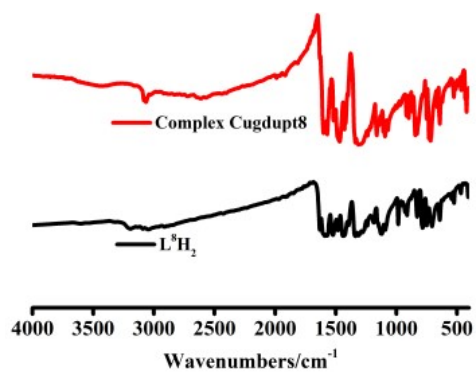


Fig. S23. IR (KBr) spectra of **Cugdup8** and  $L^8H_2$ .

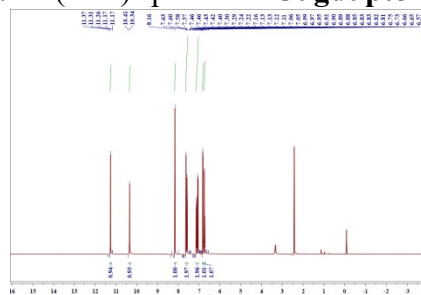


Fig. S24.  $^1H$  NMR (500MHz, DMSO- $d_6$ ) for  $L^8H_2$ .

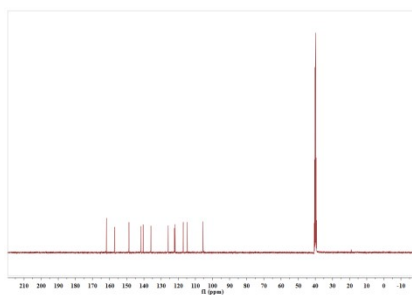


Fig. S25.  $^{13}C$  NMR (500MHz, DMSO- $d_6$ ) for  $L^8H_2$ .

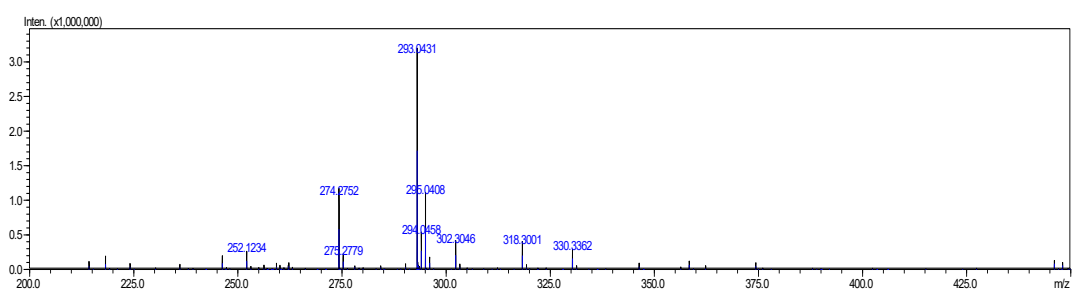


Fig. S26. ESI-MS spectra of  $L^8H_2$ .

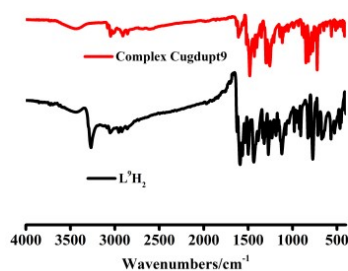


Fig. S27. IR (KBr) spectra of **Cugdup9** and  $L^9H_2$ .

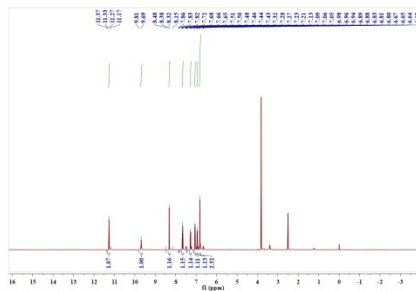


Fig. S28.  $^1\text{H}$  NMR (500MHz, DMSO- $d_6$ ) for  $\text{L}^9\text{H}_2$ .

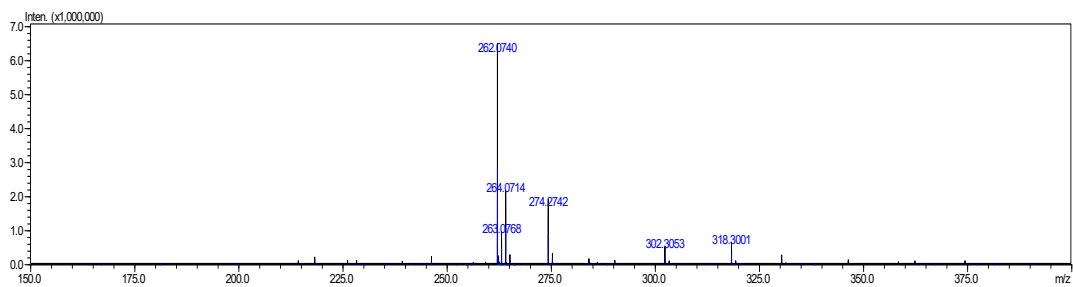


Fig. S29. ESI-MS spectra of  $\text{L}^9\text{H}_2$ .

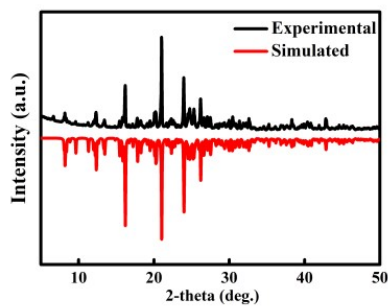


Fig. S30. XRD of the complex  $\text{Cugdupt1}$ .

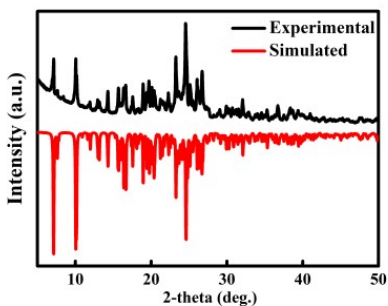


Fig. S31. XRD of the complex  $\text{Cugdupt2}$ .

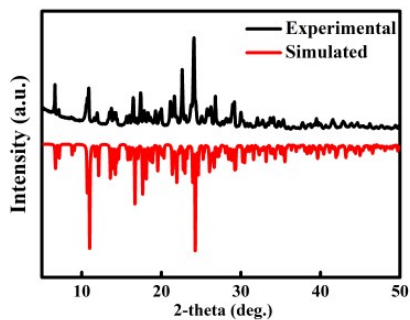


Fig. S32. XRD of the complex  $\text{Cugdupt3}$ .

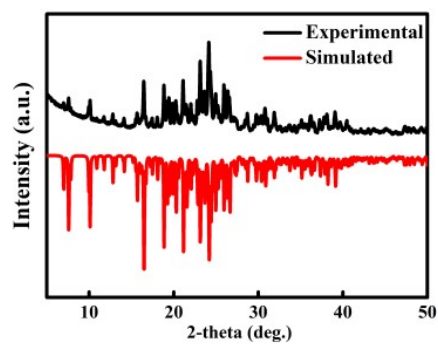


Fig. S33. XRD of the complex Cugdupt4.

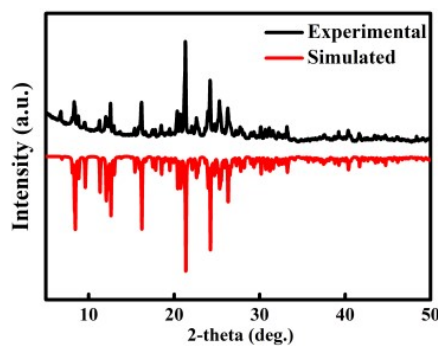


Fig. S34. XRD of the complex Cugdupt5.

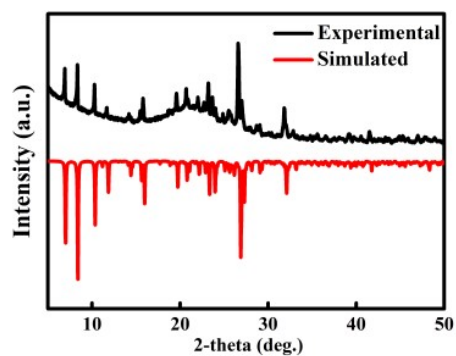


Fig. S35. XRD of the complex Cugdupt6.

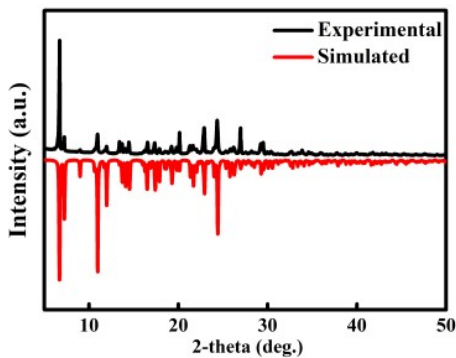
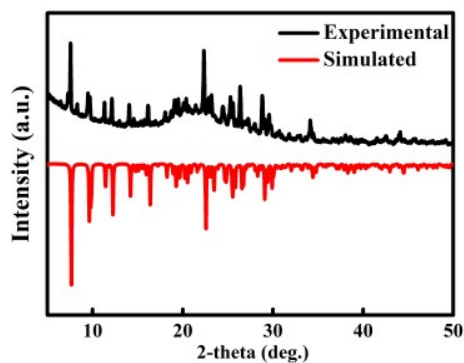
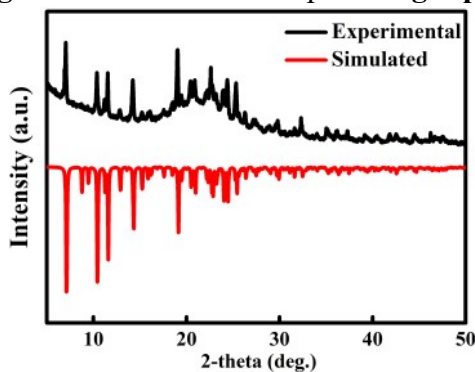


Fig. S36. XRD of the complex Cugdupt7.



**Fig. S37.** XRD of the complex **Cugdupt8**.



**Fig. S38.** XRD of the complex **Cugdupt9**.

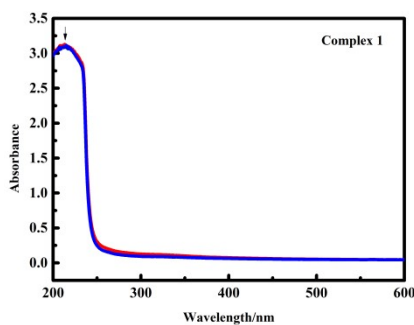


**Fig. S39.** UV-Vis absorption spectra of the complex **Cugdupt1** (50  $\mu\text{mol/L}$ ) in Tris-HCl pH=7.35 buffer at different time interval(0,24,48h).

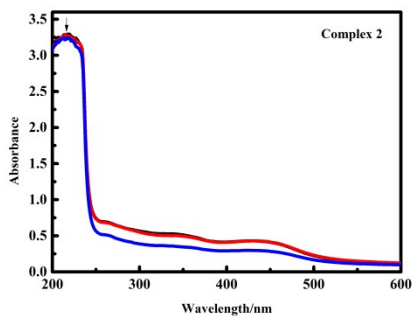


**Fig. S40.** UV-Vis absorption spectra of the complex **Cugdupt2** (50  $\mu\text{mol/L}$ ) in Tris-HCl pH=7.35 buffer at different time interval(0,24,48h).

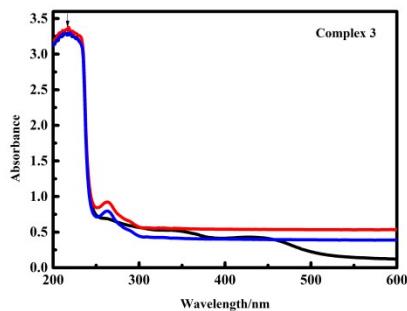


**Fig. S41.** UV-Vis absorption spectra of the complex **Cugdupt3**(50  $\mu\text{mol/L}$ ) in Tris-HCl pH=7.35 buffer at different time interval(0,24,48h).

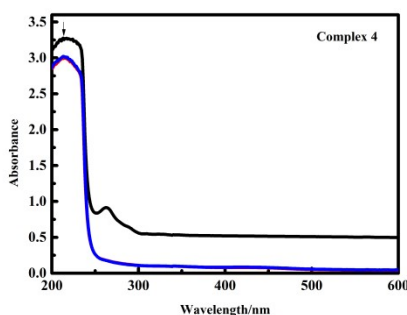


**Fig. S42.** UV-Vis absorption spectra of the complex **Cugdupt4**(50  $\mu\text{mol/L}$ ) in Tris-HCl pH=7.35 buffer at different time interval(0,24,48h).

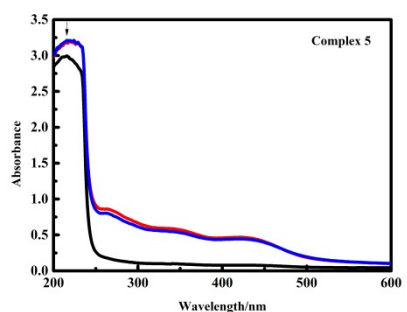


**Fig. S43.** UV-Vis absorption spectra of the complex **Cugdupt5**(50  $\mu\text{mol/L}$ ) in Tris-HCl pH=7.35 buffer at different time interval(0,24,48h).

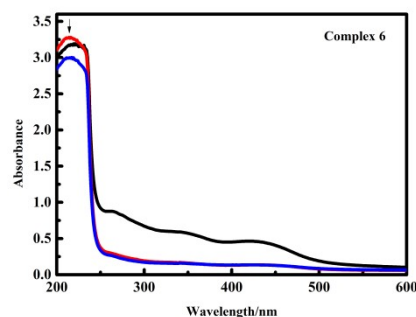


**Fig. S44.** UV-Vis absorption spectra of the complex **Cugdupt6**(50  $\mu\text{mol/L}$ ) in Tris-HCl pH=7.35 buffer at different time interval(0,24,48h).

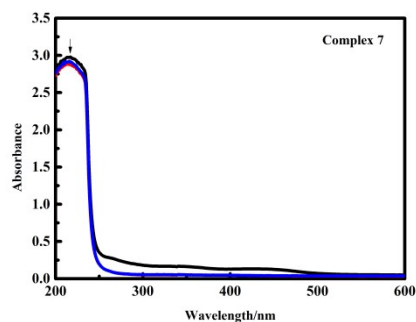


**Fig. S45.** UV-Vis absorption spectra of the complex **Cugdupt7**(50  $\mu\text{mol/L}$ ) in Tris-HCl pH=7.35 buffer at different time interval(0,24,48h).

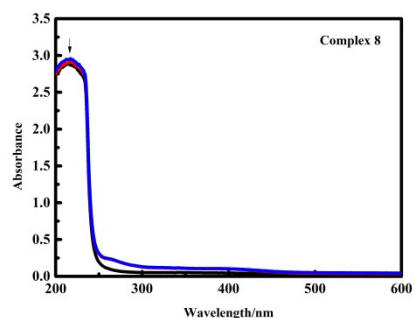


**Fig. S46.** UV-Vis absorption spectra of the complex **Cugdupt8**(50  $\mu\text{mol/L}$ ) in Tris-HCl pH=7.35 buffer at different time interval(0,24,48h).

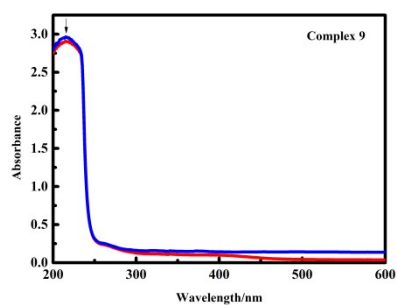


**Fig. S47.** UV-Vis absorption spectra of the complex **Cugdupt9**(50  $\mu\text{mol/L}$ ) in Tris-HCl pH=7.35 buffer at different time interval(0,24,48h).

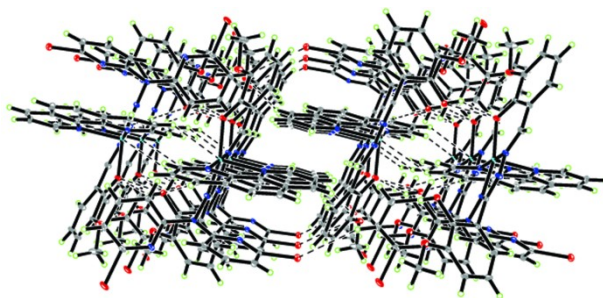


**Figure S48.** 3D network of **Cugdupt3**.

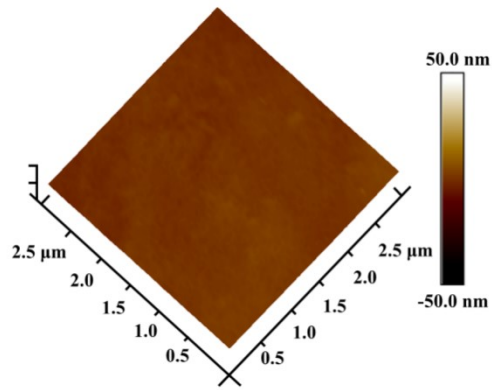


**Figure S49.** AFM image of the **Cugdupt8**.

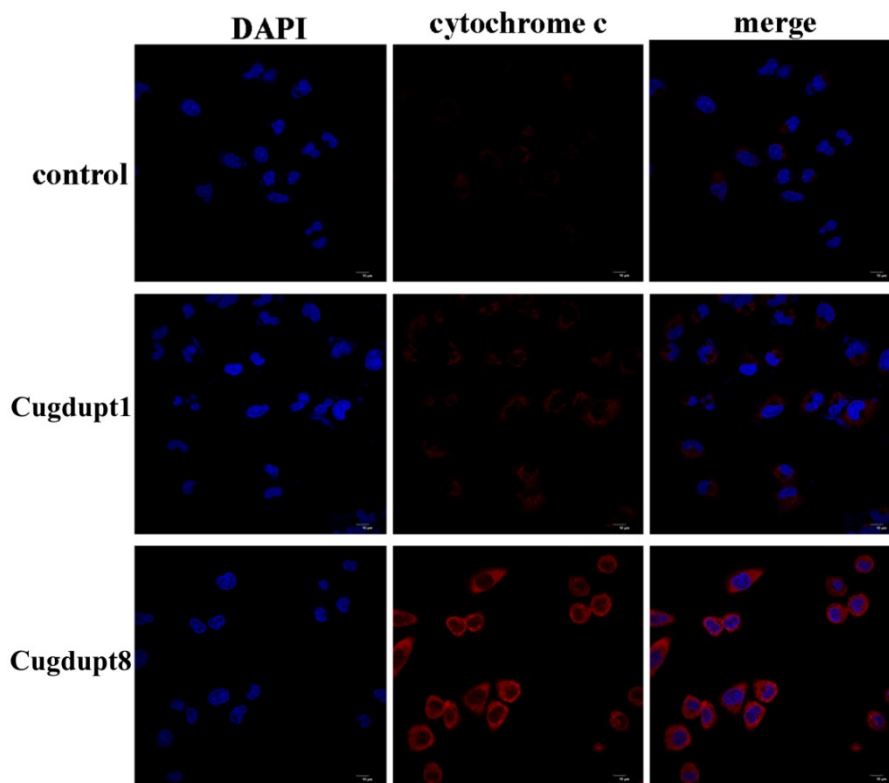


**Figure S50.** The level of cytochrome c in A549cis cells with **Cugdupt8** ( $0.5\mu\text{M}$ ) and **Cugdupt1** ( $10.0\mu\text{M}$ ) for 24 h.

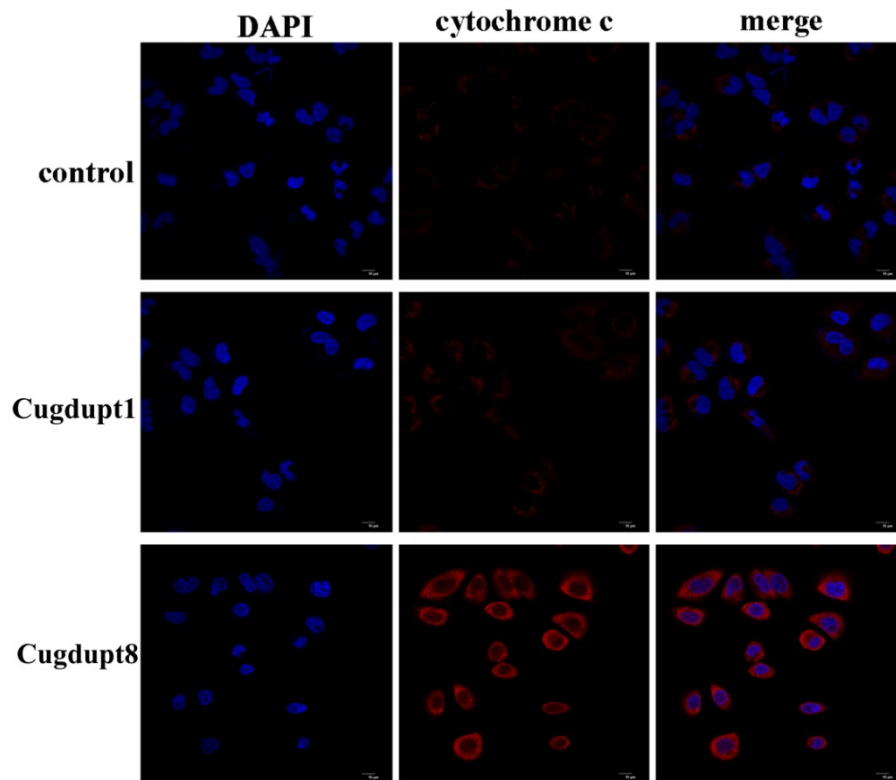


**Figure S51.** The level of cytochrome c in A549cis cells with **Cugdupt8** (0.5 $\mu$ M) and **Cugdupt1** (10.0 $\mu$ M) for 24 h.

**Table S1.** Crystallographic data for **Cugdupt1-9.**

Complex	<b>Cugdupt1</b>	<b>Cugdupt2</b>	<b>Cugdupt3</b>	<b>Cugdupt4</b>	<b>Cugdupt5</b>	<b>Cugdupt6</b>	<b>Cugdupt7</b>	<b>Cugdupt8</b>	<b>Cugdupt9</b>
Formula	C <sub>36</sub> H <sub>22</sub> Br <sub>4</sub> CuN <sub>8</sub> O <sub>2</sub>	C <sub>38</sub> H <sub>21</sub> Br <sub>2</sub> Cl <sub>4</sub> CuN <sub>9</sub> O <sub>2</sub>	C <sub>38</sub> H <sub>28</sub> Br <sub>2</sub> CuN <sub>8</sub> O <sub>2</sub>	C <sub>38</sub> H <sub>22</sub> Br <sub>6</sub> CuN <sub>9</sub> O <sub>2</sub>	C <sub>36</sub> H <sub>22</sub> Br <sub>2</sub> Cl <sub>2</sub> CuN <sub>8</sub> O <sub>2</sub>	C <sub>36</sub> H <sub>20</sub> Cl <sub>6</sub> CuN <sub>8</sub> O	C <sub>38</sub> H <sub>28</sub> Cl <sub>2</sub> CuN <sub>8</sub> O <sub>4</sub>	C <sub>36</sub> H <sub>22</sub> Cl <sub>2</sub> CuN <sub>10</sub> O <sub>6</sub>	C <sub>38</sub> H <sub>28</sub> Cl <sub>2</sub> CuN <sub>8</sub> O <sub>2</sub>
<i>Mr</i>	981.80	1001.81	884.04	1179.64	892.87	872.84	795.12	825.07	771.12
Crystal size (mm)	0.18×0.15×0.12	0.22×0.20×0.18	0.18×0.15×0.12	0.20×0.18×0.16	0.20×0.18×0.17	0.22×0.20×0.21	0.20×0.18×0.16	0.21×0.18×0.15	0.20×0.18×0.16
Crystal system	Triclinic	Monoclinic	Monoclinic	Monoclinic	Triclinic	Monoclinic	Triclinic	Monoclinic	Monoclinic
Space group	<i>P</i> $\bar{1}$	<i>I</i> 2/a	<i>P</i> 2 <sub>1</sub> / <i>c</i>	<i>I</i> 2/a	<i>P</i> $\bar{1}$	<i>I</i> 2/a	<i>P</i> 2 <sub>1</sub> / <i>c</i>	<i>P</i> 2 <sub>1</sub> / <i>c</i>	<i>P</i> 2 <sub>1</sub> / <i>n</i>
<i>a</i> (Å)	11.4205(11)	23.4053(15)	13.4524(5)	22.763(3)	11.4592(10)	12.9685(17)	13.5505(9)	18.6784(3)	15.6984(7)
<i>b</i> (Å)	12.1977(11)	14.7639(8)	10.6152(4)	15.0213(12)	12.1673(11)	14.0639(16)	10.7298(9)	15.0262(2)	11.6109(5)
<i>c</i> (Å)	14.9072(13)	22.8746(16)	25.0931(8)	23.524(3)	14.7545(14)	39.685(4)	25.0311(19)	11.98410(10)	20.2139 (11)
$\alpha$ (°)	111.137(4)	90	90.00	90	111.949(4)	90.00	90	90	90
$\beta$ (°)	102.735(4)	97.788(6)	101.312(3)	98.088(11)	103.209(4)	95.558(10)	102.958(7)	104.9810(10)	90.498
$\gamma$ (°)	102.469(4)	90	90.00	90	103.135(4)	90.00	90	90	90
<i>V</i> (Å <sup>3</sup> )	1786.9(3)	7831.5(9)	3513.7(2)	7963.5(15)	1742.7(3)	7204.1(15)	3546.7(5)	3249.20(7)	3684.3 (3)
<i>F</i> (000)	958	3768	1772	4544	886	3512	1628	1676	1580
<i>Z</i>	2	8	4	8	2	8	4	4	4
<i>D</i> <i>c</i> (g cm <sup>-3</sup> )	1.825	1.699	1.671	1.968	1.702	1.610	1.489	1.687	1.390
$\mu$ (mm <sup>-1</sup> )	5.129	2.92	5.416	6.617	3.120	1.099	0.82	4.982	0.785
$\theta$ range (°)	2.61, 27.58	2.34, 25.00	2.913, 60.286	2.332, 25.498	2.04, 24.999	2.897, 24.999	3.09, 25.00	2.13, 60.14	2.41, 25.05
Ref. meas. / indep.	57211/8213	12775,6890	26886,7781	13666,7048	41651/6134	12897/6338	12992/6216	22218/7231	11361/6160
Obs. ref. [ <i>I</i> > 2 $\sigma$ ( <i>I</i> )]	5932	4393	6894	2091	5779	2916	4051	6514	4617
<i>R</i> <sub>int</sub>	0.0710	0.0421	0.0307	0.1542	0.0809	0.1014	0.0475	0.0327	0.0302
<i>R</i> <sub>1</sub> [ <i>I</i> ≥ 2 $\sigma$ ( <i>I</i> )] <sup>a</sup>	0.0419	0.0477	0.0339	0.0850	0.0385	0.0672	0.0480	0.0371	0.0562
$\omega R_2$ (all data) <sup>b</sup>	0.1092	0.1327	0.0800	0.2448	0.1036	0.1404	0.1367	0.087	0.1958
Goof	1.002	0.992	0.99	0.951	0.099	0.96	0.999	0.996	0.998
$\Delta\rho$ (max,min)(e Å <sup>-3</sup> )	0.79, -0.99	0.56,-0.39	0.58,-0.56	0.79,-0.52	0.47, -0.67	0.43,-0.42	0.49, -0.49	0.61, -0.35	0.88,-0.47

<sup>a</sup>  $RI = \sum |F_o| - |F_c| / \sum |F_o|$ . <sup>b</sup>  $wR2 = [\sum w(|F_o^2| - |F_c^2|)^2 / \sum w(|F_o^2|)^2]^{1/2}$

**Table S2.** Selected bond lengths (Å) and bond angles (°) for **Cugdupt1-9**

bond lengths	<b>Cugdupt1</b>	<b>Cugdupt2</b>	<b>Cugdupt3</b>	<b>Cugdupt4</b>	<b>Cugdupt5</b>	<b>Cugdupt6</b>	<b>Cugdupt7</b>	<b>Cugdupt8</b>	<b>Cugdupt9</b>
Cu1-O1	1.928(2)	1.907(3)	1.9397(16)	1.912(11)	1.933(2)	1.942(4)	1.942(3)	1.9382(14)	1.947(3)
Cu1-N1	2.272(3)	2.018(4)	2.0119(19)	1.982(14)	2.050(3)	2.233(5)	2.248(3)	2.0516(16)	2.052(3)
Cu1-N2	2.048(3)	2.301(4)	2.2373(18)	2.326(14)	2.269(3)	2.053(5)	2.022(3)	2.2575(17)	2.256(4)
Cu1-N3	1.935(3)	1.926(4)	1.9417(19)	1.931(13)	1.931(2)	1.945(5)	1.943(3)	1.9502(16)	1.952(3)
Cu1-N5	1.977(3)	1.960(4)	1.9453(18)	1.935(14)	1.979(3)	1.969(5)	1.943(3)	1.9618(17)	1.940(4)
bond angles									
O1-Cu1-N1	95.59(12)	91.66 (15)	91.12(7)	92.2(5)	90.85(10)	96.4(2)	94.92(12)	91.78(6)	93.73(13)
O1-Cu1-N2	90.63(11)	90.14(15)	94.31(7)	89.3(5)	95.37(11)	90.25(18)	91.29(12)	97.26(6)	94.40(15)
O1-Cu1-N3	92.41(11)	92.14(15)	91.66(7)	92.4(5)	92.35(10)	91.9(2)	91.50(12)	92.46(6)	92.27(13)
O1-Cu1-N5	165.27(11)	166.24(15)	161.69(8)	166.1(5)	166.31(10)	166.1(2)	161.35(13)	167.66(7)	157.47(15)
N5-Cu1-N1	98.69(12)	95.58(15)	97.26(7)	95.9(5)	95.47(10)	96.3(2)	102.78(13)	94.65(7)	96.04(14)
N5-Cu1-N2	96.05(11)	102.86(15)	103.23(7)	103.5(5)	97.79(10)	97.9(2)	97.89(13)	74.41(6)	107.54(15)
N2-Cu1-N1	76.99(13)	77.10(16)	79.00(7)	77.2(6)	76.88(12)	77.8(2)	78.50(13)	77.62(6)	77.15(14)
N3-Cu1-N5	79.44(11)	80.07(15)	79.18(8)	79.1(5)	79.54(11)	78.8(2)	78.50(13)	79.04(7)	78.09(14)
N3-Cu1-N1	109.70(13)	175.07(16)	175.77(7)	174.6(6)	170.25(12)	108.6(2)	104.55(13)	166.81(7)	173.96(14)
N3-Cu1-N2	172.31(13)	106.04(16)	103.95(7)	105.5(6)	111.95(12)	173.0(2)	175.66(14)	114.17(6)	103.12(15)

**Table S3.** The tumor volume (cm<sup>3</sup>) in **Cugdupt8** treated and non-treated mice from the date of surgery to the study end point in the A549-xenograft model (mean±SD, n=6).

	1day	3day	5day	7day	9day	11day	13day	15day	17day	19day	21day
control	0.09±0.004	0.133±0.004	0.232±0.007	0.301±0.02	0.42±0.018	0.569±0.021	0.651±0.031	0.756±0.035	0.829±0.047	0.902±0.055	1.017±0.08
<b>Cugdupt8</b>	0.092±0.006	0.121±0.011	0.192±0.016	0.227±0.016	0.273±0.02	0.326±0.018	0.352±0.014	0.383±0.027	0.396±0.031	0.419±0.031	0.45±0.04

\*  $p < 0.01$ ,  $p$  vs vehicle control.

**Table S4.** Average body weight (g) in **Cugdupt8** treated and non-treated mice from the date of surgery to the study end point in the A549-xenograft model (mean±SD, n=6).

	1day	3day	5day	7day	9day	11day	13day	15day	17day	19day	21day
control	18.8±0.4	19±0.4	19.3±0.5	19.5±0.5	19.8±0.5	19.9±0.5	20.2±0.5	20.4±0.5	20.6±0.5	20.9±0.5	21.1±0.5
<b>Cugdupt8</b>	18.9±0.4	19.1±0.4	19.4±0.4	19.7±0.5	19.9±0.5	20.1±0.6	20.4±0.7	20.6±0.7	20.8±0.7	21.1±0.7	21.3±0.8

\*  $p < 0.01$ ,  $p$  vs vehicle control.

**Table S5.** In vivo anti-cancer activity of **Cugdupt8** (5.0 mg/kg) toward A549-tumor xenograft (mean±SD, n=6).

	average tumor weight (mean ± SD, g)	inhibition of tumor growth (%)
control	1.13±0.06	--
<b>Cugdupt8</b>	0.49±0.03	56.9

\*  $p < 0.01$ ,  $p$  vs vehicle control.

## Anticancer activity in vivo

When A549 tumors reach a volume of 0.09-0.10 cm<sup>3</sup> on all mice, the mice were randomized into vehicle control and treatment groups (n=6/group), received the following treatments: (a) vehicle control, 5.0% v/v DMSO/ saline vehicle, (b) complex at dose 5.0 mg/kg every two day (5.0% v/v DMSO/saline). The tumor volumes were determined every two days by measuring length (*l*) and width (*w*) and calculating volume, tumor volume and inhibition of tumor growth were calculated using formulas 1–3:

$$\text{Tumor volume: } V = (w^2 \times l) / 2 \quad (1)$$

$$\text{The tumor relative increment rate: } T/C (\%) = T_{RTV} / C_{RTV} \times 100\% \quad (2)$$

$$\text{inhibition of tumor growth: } IR(\%) = (W_c - W_t) / W_c \times 100\% \quad (3)$$

Where *w* and *l* mean the shorter and the longer diameter of the tumor respectively;  $T_{RTV}$  and  $C_{RTV}$  was the RTV of treated group and control group respectively. (RTV: relative tumor volume,  $RTV = V_t / V_0$ );  $W_t$  and  $W_c$  mean the average tumor weight of complex-treated and vehicle group respectively.

In addition, the A549 xenograft mouse models were purchased from Shanghai Lingchang Biotechnology Company Limited (Shanghai, China, approval No. SCXK (Hu) 2018-0003). The animal procedures were approved by Nanjing Ramda Pharmaceutical Co., Ltd. (Jiangsu, China, approval No. SYXK(Su) 2022-0038). And all of the experimental procedures were carried out in accordance with the NIH Guidelines for the Care and Use of Laboratory Animals. The animal experiments were approved by Nanjing Ramda Pharmaceutical Co., Ltd. (Jiangsu, China).

## Statistical Analysis

The experiments have been repeated from three to five times, and the results obtained are presented as means  $\pm$  standard deviation (SD). Significant changes were assessed by using Student's *t* test for unpaired data, and *p* values of <0.05 or <0.01 were considered significant.